Viscous-to-viscoelastic transition in phononic crystal and metamaterial band structures

Michael J. Frazier and Mahmoud I. Hussein[a)]
Department of Aerospace Engineering Sciences, University of Colorado Boulder, Boulder, Colorado 80309, USA

(Received 3 March 2015; revised 8 September 2015; accepted 16 October 2015; published online 19 November 2015)

The dispersive behavior of phononic crystals and locally resonant metamaterials is influenced by the type and degree of damping in the unit cell. Dissipation arising from viscoelastic damping is influenced by the past history of motion because the elastic component of the damping mechanism adds a storage capacity. Following a state-space framework, a Bloch eigenvalue problem incorporating general viscoelastic damping based on the Zener model is constructed. In this approach, the conventional Kelvin–Voigt viscous-damping model is recovered as a special case. In a continuous fashion, the influence of the elastic component of the damping mechanism on the band structure of both a phononic crystal and a metamaterial is examined. While viscous damping generally narrows a band gap, the hereditary nature of the viscoelastic conditions reverses this behavior. In the limit of vanishing heredity, the transition between the two regimes is analyzed. The presented theory also allows increases in modal dissipation enhancement (metadamping) to be quantified as the type of damping transitions from viscoelastic to viscous. In conclusion, it is shown that engineering the dissipation allows one to control the dispersion (large versus small band gaps) and, conversely, engineering the dispersion affects the degree of dissipation (high or low metadamping).
 [http://dx.doi.org/10.1121/1.4934845]

[ANN] Pages: 3169–3180

I. INTRODUCTION

The field of wave propagation in periodic materials has witnessed an explosive increase in activity over the past few decades,[1] especially in the category of phononic crystals[2,3] and acoustic/elastic metamaterials,[4] collectively, phononic materials. The appeal of intrinsic vibration control by design gives impetus to phononic materials research. However, despite its physical importance, there are only a few investigations into the impact of material damping on wave propagation. Nevertheless, discrepancies between theoretical and experimental results in some studies have been attributed to energy loss, e.g., Ref. 5. The theoretical acknowledgment of dissipative effects not only constitutes a more authentic description of the dispersion characteristics of phononic materials, but also provides a means by which the material design process may be guided by the application-specific demand for the maximization (or minimization) of dissipation.[6]

Of the studies that consider the treatment of damping, many focus on simulating finite periodic structures.[7–9] Dispersion analysis at the unit cell level, on the other hand, provides information on the intrinsic dynamical properties of the medium, which offers insights that are in principle applicable to any finite-structure analysis, regardless of the size, number of cells, boundary conditions, or nature of excitation. In unit cell analysis, wave propagation in a periodic material is fully characterized by the application of Bloch's theorem.[10] The proposition maintains that the wave field in a periodic medium is the product of an amplitude function with the spatial periodicity, $\mathbf{a}$, of the unit cell and a plane wave envelope. In terms of the displacement response vector, $\bar{\mathbf{u}}(\mathbf{x},\boldsymbol{\kappa},t)$, this is expressed as

$$\bar{\mathbf{u}}(\mathbf{x},\boldsymbol{\kappa},t)=\tilde{\mathbf{u}}(\mathbf{x})e^{i\boldsymbol{\kappa}\cdot\mathbf{x}+\lambda t}, \tag{1}$$

where $\tilde{\mathbf{u}}(\mathbf{x})$ represents the amplitude function that is periodic across the unit cell domain. Subsequently,

$$\bar{\mathbf{u}}(\mathbf{x}+\mathbf{a},\boldsymbol{\kappa},t)=\bar{\mathbf{u}}(\mathbf{x},\boldsymbol{\kappa},t)e^{i\boldsymbol{\kappa}\cdot\mathbf{a}}. \tag{2}$$

The wavevector, $\boldsymbol{\kappa}$, and the quantity, λ, modulate the wave envelope in space and time, respectively. In much of the literature, λ is prescribed as an imaginary value, i.e., $\lambda=-i\omega$, representing waves that decay in space but not in time when energy dissipation is present.[11–15] In the laboratory, this scenario is analogous to a harmonic (driven) excitation of a corresponding finite periodic structure. In this paper, we consider the case where λ is generally a complex number thus the energy loss manifests as temporal attenuation.[15–18] This treatment is consistent with results obtained from free vibration analysis of a corresponding damped finite periodic structure. Only in the absence of energy dissipation do the free and harmonic wave conditions yield identical results.[1]

A literature synopsis of past studies that investigated dispersion properties of damped periodic materials reveals a variety of approaches in both the manner of modeling the damping and the method of solution. Among the early studies is Mead's calculation of the wave motion phase and attenuation constants for one-dimensional (1D) lumped-parameter, chain-like models exhibiting structural damping (i.e., velocity-independent damping forces).[12] Generally, it

a)Electronic mail: mih@colorado.edu

is common to incorporate the damping via a complex elastic modulus[8,19,20] or a convolution integral expression applied to the elastic modulus.[21] Damping has also been introduced via a complex inertial term[22] and as a standalone parameter, or matrix, that multiplies with the velocity vector in the equation of motion.[17,18] The quality of an adopted damping model improves whenever its performance is compared and calibrated with experimental results.[23–25] Nevertheless, regardless of the choice, any damping model is acceptable in principle provided the resulting rate of energy dissipation is positive.[26–28]

Other than the manner of introducing the damping into the problem, a key classification of damping is in the nature of the dissipation mechanism it permits. Here, we consider two key classes: *viscous damping* and *viscoelastic damping*. Dissipation arising from viscous damping depends upon the instantaneous modal velocities. On the other hand, dissipation arising from viscoelastic damping is influenced by the past history of motion; this is because the elastic component of the damping adds a storage capacity. A viscous damping model is appropriate for material systems where fluid viscosity is the dominant dissipative mechanism, such as in a dashpot or in a configuration where the material is exposed to a fluid.[29] A viscoelastic model, on its part, is representative of a solid exhibiting material loss, such as in polymers, or generally a material that exhibits the irreversible micromechanical processes of relaxation. Non-conservative forces in a viscoelastic model are hereditarily dependent upon the entire history of motion up to and including the present state. Mathematically, this dependence manifests as a convolution integral over kernel functions rather than the instantaneous value of any state variable. The contrast between the viscous and the viscoelastic nature of material damping results in fundamental differences in the dispersion behavior, which is the main focus of this paper.

Another aim of this work is to consider the effect of the type of damping on the dissipative capacity of phononic crystals and metamaterials, particularly the latter. One of the aims of vibration control is to decrease transmission from the environment to a protected structure. This is often attempted through the introduction of an intervening, dissipative material such as rubber. However, dissipative materials generally lack a load-bearing capacity (stiffness) and efforts to combat this deficiency usually sacrifice the damping quality that was the original appeal, revealing an age-old trade-off in materials engineering. The challenge of achieving simultaneously high stiffness and high damping within a single material has been addressed in a variety of ways using composites.[30–33] In a recent study of damped phononic materials,[6] the concept of *metadamping* was introduced to describe the notion of an amplification of dissipation in locally resonant metamaterials when compared to Bragg-scattering materials of equivalent stiffness and equally prescribed viscous damping. In the present paper, using a phononic crystal and metamaterials as Bragg and locally resonant materials, respectively, we investigate the metadamping phenomenon within the framework of both types of damping, viscous and viscoelastic.

The paper is divided into three parts, all focused on free wave motion. First, in Sec. II, we introduce the viscous and viscoelastic damping models that form the foundation of the rest of the paper; we discuss their physical attributes as it relates to material deformation and address the non-standard eigenvalue problem that arises from their representation in the equations of motion. Following this discussion, Sec. III presents wave dissipation in phononic crystals and acoustic metamaterials with a focus on the qualitative differences between the viscous and viscoelastic types. In Sec. IV, these differences are explored further to reveal the implications on metadamping. Finally, conclusions are presented in Sec. V.

II. STATE-SPACE TRANSFORMATION

Damping dependent upon state variables other than the instantaneous displacement or acceleration does not immediately yield a standard eigenvalue problem. In this section, by a state-space transformation of the equations of motion, a standard eigenvalue problem is formulated.[18,28,34] In the case of viscous damping, this transformation adopts the familiar Duncan form. For the viscoelastic description, this formulation is extended by the addition of one or more internal variables.

A. Formulation of viscous wave propagation problem

Consider the unit cell of a phononic material with spatial periodicity in one, two, or three dimensions. For a material model represented by a lumped-parameter system or by the spatial discretization of a continuum, the equations of motion for a viscously damped unit cell are written compactly in matrix form as

$$\mathbf{M}\ddot{\mathbf{u}} + \mathbf{C}\dot{\mathbf{u}} + \mathbf{K}\mathbf{u} = \mathbf{f}, \tag{3}$$

where $\mathbf{M}$, $\mathbf{C}$, and $\mathbf{K}$ are the assembled $n \times n$ mass, damping, and equilibrium stiffness matrices, respectively. While the material properties make the determination of $\mathbf{M}$ and $\mathbf{K}$ relatively straightforward, the coefficients of $\mathbf{C}$ must be extracted from experimental data.[24–26] Often, $\mathbf{C}_j$ is obtained for each material/structural constituent j so that $\mathbf{C}$ is assembled from the individual $\mathbf{C}_j$. The $n \times 1$ vector $\mathbf{u}$ collects the displacement degrees of freedom while the associated nodal forces (applied by neighboring unit cells) are contained within $\mathbf{f}$.

We define an $m \times 1$ $(m < n)$ condensed displacement vector $\hat{\mathbf{u}}$ containing the minimal set of degrees of freedom including the internal $\mathbf{u}_\mathrm{i}$ and the essential boundary $\mathbf{u}_\mathrm{b}$ displacements. The remaining boundary displacements are obtained from the essential boundary freedoms through the application of the appropriate lattice propagation constant. Thus, exploiting Eq. (2), the condensed set relates to the full set of unit-cell displacements according to $\mathbf{u} = \mathbf{T}\hat{\mathbf{u}}$, where $\mathbf{T}$ is the $n \times m$ transformation matrix enforcing the Bloch boundary conditions. For convenience, we adopt the partitioning $\hat{\mathbf{u}} = [\mathbf{u}_\mathrm{i}\ \mathbf{u}_\mathrm{b}]^\mathrm{T}$. Given this arrangement, $\mathbf{T}$ may be partitioned into suitably sized identity matrices $\mathbf{I}$ and diagonal matrices for each propagation direction. For the case of a cubic unit cell with lattice periods a_i $(i = 1, 2, 3)$, $\mathbf{T}$ has the block form

$$\mathbf{T} = \begin{bmatrix} \mathbf{I} & \mathbf{0} \\ \mathbf{0} & \mathbf{I} \\ \mathbf{0} & \mathbf{I}e^{i\kappa_1 a_1} \\ \mathbf{0} & \mathbf{I}e^{i\kappa_2 a_2} \\ \mathbf{0} & \mathbf{I}e^{i\kappa_3 a_3} \\ \mathbf{0} & \mathbf{I}e^{i(\kappa_1 a_1+\kappa_2 a_2)} \\ \mathbf{0} & \mathbf{I}e^{i(\kappa_2 a_2+\kappa_3 a_3)} \\ \mathbf{0} & \mathbf{I}e^{i(\kappa_1 a_1+\kappa_3 a_3)} \\ \mathbf{0} & \mathbf{I}e^{i\boldsymbol{\kappa}\cdot\mathbf{a}} \end{bmatrix}. \tag{4}$$

Equation (3) is written in terms of $\hat{\mathbf{u}}$ as follows:

$$\hat{\mathbf{M}}\ddot{\hat{\mathbf{u}}} + \hat{\mathbf{C}}\dot{\hat{\mathbf{u}}} + \hat{\mathbf{K}}\hat{\mathbf{u}} = \mathbf{0}, \tag{5}$$

where

$$\hat{\mathbf{M}} = \mathbf{T}^*\mathbf{M}\mathbf{T}, \tag{6a}$$

$$\hat{\mathbf{C}} = \mathbf{T}^*\mathbf{C}\mathbf{T}, \tag{6b}$$

$$\hat{\mathbf{K}} = \mathbf{T}^*\mathbf{K}\mathbf{T}, \tag{6c}$$

and $\mathbf{T}^*\mathbf{f} = \mathbf{0}$,[35] with $\mathbf{T}^*$ being the conjugate transpose of $\mathbf{T}$. Although, in this work, the Bloch condition is applied through $\mathbf{T}$, alternative formulations for lumped-parameter[34] and discretized[17,18,36] systems are suitable. One benefit of the formulation is that it brings lumped-parameter and finite-element (FE) models under the same treatment. In this two-step approach, one first formulates the structural matrices of the lumped or FE model, and then applies the boundary transformation matrix $\mathbf{T}$.

Equation (5) formulates a coupled, non-standard eigenvalue problem with eigenvalues λ_s and eigenvectors $\hat{\mathbf{u}}_s$ ($s = 1, \ldots, m$). However, the matrix $\hat{\mathbf{C}}$ is generally not diagonalizable with eigenvectors associated with $\hat{\mathbf{M}}$ and $\hat{\mathbf{K}}$. Thus, we recast Eq. (5) into first-order form via a state-space transformation[18]

$$\hat{\mathbf{A}}\dot{\hat{\mathbf{y}}} + \hat{\mathbf{B}}\hat{\mathbf{y}} = \mathbf{0}, \tag{7}$$

where

$$\hat{\mathbf{A}} = \begin{bmatrix} \mathbf{0} & \hat{\mathbf{M}} \\ \hat{\mathbf{M}} & \hat{\mathbf{C}} \end{bmatrix}, \tag{8a}$$

$$\hat{\mathbf{B}} = \begin{bmatrix} -\hat{\mathbf{M}} & \mathbf{0} \\ \mathbf{0} & \hat{\mathbf{K}} \end{bmatrix}, \tag{8b}$$

$$\hat{\mathbf{y}} = [\dot{\hat{\mathbf{u}}}\ \hat{\mathbf{u}}]^{\mathrm{T}}. \tag{8c}$$

Now, assuming a solution $\hat{\mathbf{y}} = \bar{\mathbf{y}}e^{\gamma t}$, we obtain a standard eigenvalue problem for which the eigenvectors are orthogonal with respect to the transformed state-space matrices.

For viscous damping, the state-space transformation doubles the size of the original problem. Consequently, the eigenvalue problem that emerges from the substitution of $\hat{\mathbf{y}} = \bar{\mathbf{y}}e^{\gamma t}$ in Eq. (7) has eigenvalues γ_s and eigenvectors $\bar{\mathbf{y}}_s$ ($s = 1, \ldots, 2m$) that appear in conjugate pairs. Given their orthogonality with respect to the system matrices, the eigenvectors decouple the equations into $2m$ modal equations with complex roots γ_s, and thus effectively represent $2m$ single-degree of freedom systems. Focusing on the members of the conjugate pair with $\mathrm{Im}[\gamma_s] > 0$, we can write

$$\begin{aligned}\gamma_s(\boldsymbol{\kappa}) &= -\zeta_s(\boldsymbol{\kappa})\omega_{\mathrm{r},s}(\boldsymbol{\kappa}) + i\omega_s(\boldsymbol{\kappa})\sqrt{1-\zeta_s^2(\boldsymbol{\kappa})} \\ &= -\zeta_s(\boldsymbol{\kappa})\omega_{\mathrm{r},s}(\boldsymbol{\kappa}) + i\omega_{\mathrm{d},s}(\boldsymbol{\kappa}),\ s = 1, \ldots, m,\end{aligned} \tag{9}$$

where, in the special case of Rayleigh (proportional) damping, $\omega_{\mathrm{r},s}(\boldsymbol{\kappa})$ is the undamped frequency. From Eq. (9), we extract the wavevector-dependent damped frequency $\omega_{\mathrm{d},s}(\boldsymbol{\kappa})$ and damping ratio $\zeta_s(\boldsymbol{\kappa})$, respectively

$$\omega_{\mathrm{d},s}(\boldsymbol{\kappa}) = \mathrm{Im}[\gamma_s(\boldsymbol{\kappa})], \tag{10}$$

$$\zeta_s(\boldsymbol{\kappa}) = -\frac{\mathrm{Re}[\gamma_s(\boldsymbol{\kappa})]}{\mathrm{Abs}[\gamma_s(\boldsymbol{\kappa})]}. \tag{11}$$

B. Formulation of viscoelastic wave propagation problem

For the case of viscous damping presented in Sec. II A, the non-conservative forces are assumed to depend only on the instantaneous velocities. In practice, this is unique to a situation in which a viscous fluid is the mechanism for dissipation. The dissipative forces within common materials such as polymers, composites, and even metals nonviscously depend on quantities other than the instantaneous velocities. In the linear hereditary theory, energy loss is attributed to the phase lag between the displacement and the internal stress.[37] The label "hereditary" refers to the role of the past history of motion on the current state. While preserving the linearity of the problem, a general way of imparting this characteristic to Eqs. (3) and (5) is through convolution integrals over kernel functions $G(t)$.[29] With exponentially decreasing kernel functions of the form $G(t) = \mu_1 e^{-\mu_2 t}$, we rewrite Eq. (5) as

$$\hat{\mathbf{M}}\ddot{\hat{\mathbf{u}}} + \sum_{j=1}^{\ell}\hat{\mathbf{C}}_j\int_0^t \mu_{1,j}e^{-\mu_{2,j}(t-\tau)}\dot{\hat{\mathbf{u}}}(\tau)d\tau + \hat{\mathbf{K}}\hat{\mathbf{u}} = \mathbf{0}, \tag{12}$$

where the summation reflects the possibility of multiple coefficient matrices and kernel functions with relaxation pairs ($\mu_{1,j}$, $\mu_{2,j}$) being required to accurately describe the behavior. Such a system is described as one of hereditary of degree ℓ. Although, for the Maxwell model of viscoelasticity, the kernel functions are traditionally associated with a stiffness matrix (effectively adding a dissipative capability), in Eq. (12), the kernel functions are associated with the damping matrix (effectively adding a storage capability). Figure 1 depicts a Maxwell element as a linear spring and a viscous dashpot arranged in series. The kernel function can be derived as[38]

$$G(t) = k_{\mathrm{M}}e^{(-k_{\mathrm{M}}/c)t}. \tag{13}$$

One may imagine that in the limit $k_{\mathrm{M}} \to \infty$, the viscous dashpot joins a rigid spring such that essentially no mechanical

energy is stored by the spring and, instead, is dissipated by the dashpot. Viscoelastic effects emerge to varying degrees if k_M has a finite, non-zero value that permits the storage of a portion of the mechanical energy supplied to the Maxwell element. In the limit $k_M \to 0$, the spring and dashpot effectively disengage and mechanical energy is neither conserved nor dissipated. Multiple Maxwell elements arranged in parallel to an equilibrium spring (Maxwell–Weichert model) may be applied to more accurately describe the material behavior.

In this section, we apply the state-space approach to Eq. (12) by introducing a set of internal variables. We develop the state-space matrices using an approach proposed for structural dynamics of finite systems;[28] here, we extend it to the analysis of the unit cell problem. The approach is specific to the case in which the magnitude of the relaxation pairs are equal (i.e., $\mu_j = \mu_{1,j} = \mu_{2,j}$). This particular form of the kernel function, possessing a unit area,

$$\int_0^\infty \mu_j e^{-\mu_j t}\, dt = 1, \tag{14}$$

allows the direct comparison of the viscous and viscoelastic cases.[27] For the special case of $\ell = 1$ and low damping such that the damped frequency is approximately equal to the undamped frequency, Ref. 27 describes a method for extracting μ_1 and $\mathbf{C}_1$ from experimental data.

First, we equate each convolution integral with an internal variable $\hat{\mathbf{p}}_j$ such that

$$\hat{\mathbf{p}}_j = \int_0^t \mu_j e^{-\mu_j(t-\tau)} \dot{\hat{\mathbf{u}}}(\tau)\, d\tau, \tag{15}$$

$$\hat{\mathbf{M}}\ddot{\hat{\mathbf{u}}} + \sum_{j=1}^{\ell} \hat{\mathbf{C}}_j \hat{\mathbf{p}}_j + \hat{\mathbf{K}}\hat{\mathbf{u}} = \mathbf{0}. \tag{16}$$

From the Leibniz integral rule applied to Eq. (15), we obtain

$$\dot{\hat{\mathbf{p}}}_j = -\int_0^t \mu_j^2 e^{-\mu_j(t-\tau)} \dot{\hat{\mathbf{u}}}(\tau) d\tau + \mu_j \dot{\hat{\mathbf{u}}} = \mu_j[\dot{\hat{\mathbf{u}}} - \hat{\mathbf{p}}_j]. \tag{17}$$

Substituting Eq. (17) into Eq. (16) gives

$$\hat{\mathbf{M}}\ddot{\hat{\mathbf{u}}} + \sum_{j=1}^{\ell} \hat{\mathbf{C}}_j \left[\dot{\hat{\mathbf{u}}} - \frac{1}{\mu_j}\dot{\hat{\mathbf{p}}}_j\right] + \hat{\mathbf{K}}\hat{\mathbf{u}} = \mathbf{0}. \tag{18}$$

At this point, incorporating Eq. (18) into a state-space format will result in non-square matrices. To produce square and block-symmetric state-space matrices, we formulate an additional equation. Premultiplying Eq. (17) by $\hat{\mathbf{C}}_j$ and dividing by μ_j^2 yields

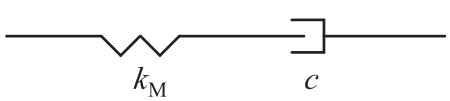

FIG. 1. Maxwell element composed of a series arrangement of a linear elastic spring and a viscous dashpot representing, respectively, conservative and non-conservative mechanical processes.

$$-\frac{1}{\mu_j}\hat{\mathbf{C}}_j\dot{\hat{\mathbf{u}}} - \frac{1}{\mu_j^2}\hat{\mathbf{C}}_j\dot{\hat{\mathbf{p}}}_j + \frac{1}{\mu_j}\hat{\mathbf{C}}_j\hat{\mathbf{p}}_j = \mathbf{0}. \tag{19}$$

Finally, adjoining Eqs. (18) and (19), we may assemble the problem into the state-space format of Eq. (7) where

$$\hat{\mathbf{A}} = \begin{bmatrix} \mathbf{0} & \hat{\mathbf{M}} & \mathbf{0} & \mathbf{0} & \cdots & \mathbf{0} \\ \hat{\mathbf{M}} & \sum_{j=1}^{\ell}\hat{\mathbf{C}}_j & -\frac{1}{\mu_1}\hat{\mathbf{C}}_1 & -\frac{1}{\mu_2}\hat{\mathbf{C}}_2 & \cdots & -\frac{1}{\mu_\ell}\hat{\mathbf{C}}_\ell \\ \mathbf{0} & -\frac{1}{\mu_1}\hat{\mathbf{C}}_1 & \frac{1}{\mu_1^2}\hat{\mathbf{C}}_1 & \mathbf{0} & \cdots & \mathbf{0} \\ \mathbf{0} & -\frac{1}{\mu_2}\hat{\mathbf{C}}_2 & \mathbf{0} & \frac{1}{\mu_2^2}\hat{\mathbf{C}}_2 & \cdots & \mathbf{0} \\ \vdots & \vdots & \vdots & \vdots & \ddots & \vdots \\ \mathbf{0} & -\frac{1}{\mu_\ell}\hat{\mathbf{C}}_\ell & \mathbf{0} & \mathbf{0} & \cdots & \frac{1}{\mu_\ell^2}\hat{\mathbf{C}}_\ell \end{bmatrix}, \tag{20a}$$

$$\hat{\mathbf{B}} = \mathrm{diag}\left[-\hat{\mathbf{M}} \quad \hat{\mathbf{K}} \quad \frac{1}{\mu_1}\hat{\mathbf{C}}_1 \quad \frac{1}{\mu_2}\hat{\mathbf{C}}_2 \quad \cdots \quad \frac{1}{\mu_\ell}\hat{\mathbf{C}}_\ell\right], \tag{20b}$$

$$\hat{\mathbf{y}} = [\dot{\hat{\mathbf{u}}}\ \hat{\mathbf{u}}\ \hat{\mathbf{p}}_1\ \hat{\mathbf{p}}_2\ \cdots\ \hat{\mathbf{p}}_\ell]^{\mathrm{T}}, \tag{20c}$$

and diag[·] contains the elements of a block diagonal matrix.

Upon obtaining the eigenvalues γ_s, there are m conjugate pairs that physically represent the modes of damped wave propagation. The remaining real eigenvalues are non-oscillating. As seen in the above formulation, in the limit $\mu_j \to \infty\ \forall j$, the viscous state-space formulation [Eq. (8)] is recovered. That is, high values of μ_j represent more viscous behavior (less dependence on the past history), while low values of μ_j represent more viscoelastic behavior (more dependence on the past history).

III. BAND STRUCTURE OF DAMPED PHONONIC MATERIALS AND THE VISCOUS-TO-VISCOELASTIC TRANSITION

A. Lumped parameter model

The formulations in Eqs. (8) and (20) are suitable to an FE discretization of a material continuum; however, for simplicity, to compare the effects of viscous and viscoelastic damping on wave propagation in periodic materials, we utilize a simple, 1D lumped-parameter material model composed of point masses, linear elastic springs, and viscous dashpots. Furthermore, we examine the results for two archetypal material configurations: phononic crystal (PC) [Figs. 2(a) and 2(c)] and acoustic metamaterial (AM) [Figs. 2(b) and 2(d)]. For the purpose of demonstration, the material parameters have the following relations: $m_2/m_1 = r_m = 3$, $c_2/c_1 = r_c = 1/2$, and $k_2/k_1 = r_k = 1$. With these criteria and degrees of freedom organized such that $\mathbf{u} = [u_1 \quad u_2 \quad u_L]^{\mathrm{T}}$, $\mathbf{f} = [f_1 \quad f_2 \quad f_L]^{\mathrm{T}}$, and $\hat{\mathbf{u}} = [u_1 \quad u_2]^{\mathrm{T}}$, we write the matrices associated with

each unit-cell configuration in Fig. 2 explicitly. The two material configurations share a common mass matrix,

$$\mathbf{M} = m_2\mathbf{M}_o = m_2\begin{bmatrix} 1/r_m & 0 & 0 \\ 0 & 1 & 0 \\ 0 & 0 & 0 \end{bmatrix}. \tag{21}$$

Specifically, for the phononic crystal,

$$\mathbf{C} = c_2\mathbf{C}_o = c_2\begin{bmatrix} 1/r_c+1 & -1 & -1/r_c \\ -1 & 1 & 0 \\ -1/r_c & 0 & 1/r_c \end{bmatrix}, \tag{22a}$$

$$\mathbf{K} = k_2\mathbf{K}_o = k_2\begin{bmatrix} 1/r_k+1 & -1 & -1/r_k \\ -1 & 1 & 0 \\ -1/r_k & 0 & 1/r_k \end{bmatrix}, \tag{22b}$$

$$\mathbf{T} = \begin{bmatrix} 1 & 0 \\ 0 & 1 \\ 0 & e^{-i\kappa a} \end{bmatrix}. \tag{22c}$$

For the metamaterial,

$$\mathbf{C} = c_2\mathbf{C}_o = c_2\begin{bmatrix} 1/r_c+1 & -1 & -1/r_c \\ -1 & 1 & 0 \\ -1/r_c & 0 & 1/r_c \end{bmatrix}, \tag{23a}$$

$$\mathbf{K} = k_2\mathbf{K}_o = k_2\begin{bmatrix} 1/r_k+1 & -1 & -1/r_k \\ -1 & 1 & 0 \\ -1/r_k & 0 & 1/r_k \end{bmatrix}, \tag{23b}$$

$$\mathbf{T} = \begin{bmatrix} 1 & 0 \\ 0 & 1 \\ e^{-i\kappa a} & 0 \end{bmatrix}. \tag{23c}$$

After applying the transformation matrix, $\hat{\mathbf{M}}$, $\hat{\mathbf{C}}$, and $\hat{\mathbf{K}}$ are the same matrices appearing in Ref. 34. Dividing by m_2, the general equations of motion are

$$\hat{\mathbf{M}}_o\ddot{\hat{\mathbf{u}}} + \beta\hat{\mathbf{C}}_o\int_0^t \mu e^{-\mu(t-\tau)}\dot{\hat{\mathbf{u}}}(\tau)\,d\tau + \omega_0^2\hat{\mathbf{K}}_o\hat{\mathbf{u}} = \mathbf{0}, \tag{24}$$

where $\beta = c_2/m_2$, which varies with c_2, is a measure of damping intensity and $\omega_0 = \sqrt{k_2/m_2}$. To demonstrate the viscoelastic case, we employ only one kernel function.

B. Phononic crystal versus metamaterial, and viscous damping versus viscoelastic damping

As we examine the frequency and damping ratio dispersion diagrams, the undamped condition, realized by setting the normalized damping intensity $\beta/\omega_0 = 0$, is represented by a black curve, while light and dark green curves represent the damping conditions $\beta/\omega_0 = 0.1$ and $\beta/\omega_0 = 0.2$, respectively. In particular, the frequency diagrams are normalized with respect to $\omega_0 = 150$ rad/s.

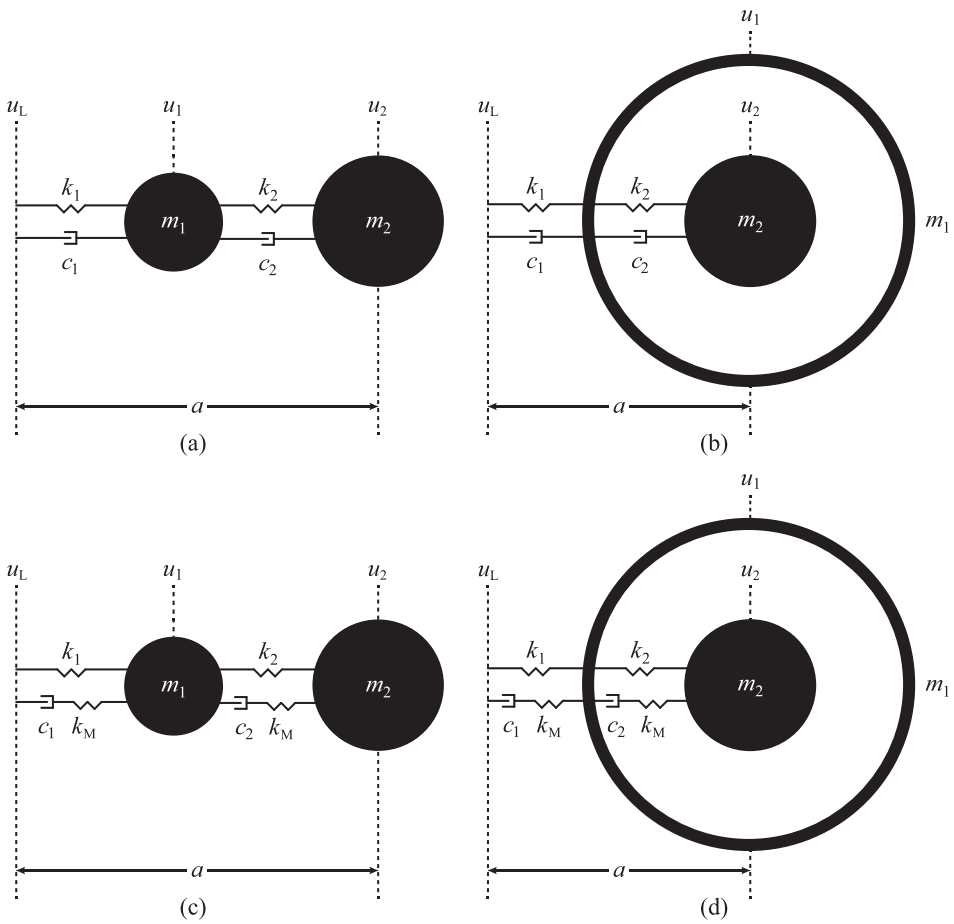

FIG. 2. Lumped parameter models of a two-mass 1D phononic material unit cell with lattice spacing a with (a),(c) the Bragg scattering configuration of a phononic crystal and (b),(d) the locally resonant configuration of an acoustic metamaterial. In (a) and (b), damping is represented by a Zener (viscoelastic damping) model, whereas in (c) and (d), it is represented by a Kelvin–Voigt (viscous damping) model.

Figures 3(a), 3(c), 3(e), and 3(g) show the dispersion diagrams generated by Eqs. (7) and (8) for the viscous case [or Eq. (20) when all the corresponding kernels are delta functions]. Because the damping force is proportional to the relative velocity (a function of λ) of each degree of freedom, the damping effect for both unit-cell configurations is more pronounced at higher frequencies. In the phononic crystal case, energy dissipated by propagating waves manifests as a decrease in propagation frequency across the whole of the wavenumber domain for each branch. Thus, the width of the band gap decreases and the value of the central frequency shifts to lower magnitudes. In the metamaterial case, on the other hand, the shift is emphasized at high-wavenumber modes. Therefore, the band gap effectively remains unchanged. The descent of the frequency band in response to material damping is consistent with the corresponding damping ratio diagrams in Figs. 3(c) and 3(g), which provide a measure of the temporal attenuation of the wave at each κ-point. In other words, for a given wavenumber, a strong shift in frequency [Figs. 3(a) and 3(e)] translates to a high value of damping ratio [Figs. 3(c) and 3(g)]. For sufficiently high damping intensity, β, overdamping [i.e., $\zeta_s(\kappa) \geq 1$] is observed over a subset of wavenumbers (not shown)—these represent non-oscillating modes (i.e., no wave motion). For these modes, wave propagation is prohibited by damping intensity, not by band-gap formation mechanisms.

Assuming a single relaxation parameter $\mu = \mu_1 = \mu_2 = 10^3$ ($k_M \propto \mu$), Figs. 3(b), 3(d), 3(f), and 3(h) demonstrate the viscoelastic case.[39] Similar to the viscous case, the effect of damping increases with frequency. However, the viscoelastic frequency diagrams in Figs. 3(b) and 3(f) display contrasting behavior compared to the viscous case. Under the chosen viscoelastic conditions, both branches show an increase in frequency across the wavenumber domain with this trait emphasized in the second branch. In analogy to the viscous case, the damping effect takes place across the entire wavenumber domain for the phononic crystal. As a consequence, the band gap widens and its central frequency shifts upward. Also in analogy to the viscous case, the frequency shift is negligible at long wavelengths for the metamaterial (at least for the chosen value of μ), causing the size and location of the band gap to remain effectively unchanged. By introducing a hereditary effect into the damping model, a portion of the mechanical energy that would be dissipated in the viscous case is instead conserved, leading to the increases in frequency and the slightly lower damping ratio values seen in Figs. 3(d) and 3(h), respectively. This is a manifestation of joining an elastic spring in series with the viscous dashpot to form a Maxwell element.

In comparing the phononic crystal and metamaterial configurations, damping, whether viscous or viscoelastic, appears to exert a profound influence over the metamaterial at high wavenumbers. This is illustrated in the band structure where equally prescribed damping intensity produces unequal changes in frequency. In Sec. IV, this phenomenon will be further explored in the context of metadamping.

While the dispersion curves in Fig. 3 show only Bloch modes corresponding to real wavenumbers, spatially attenuating modes corresponding to the band gap exist as well. These too shift due to damping as illustrated in Ref. 40, where the dispersion curves for free waves are obtained by the transfer matrix method and thus display complex wavenumbers. In the present study, the effects of damping are investigated only for propagating modes.

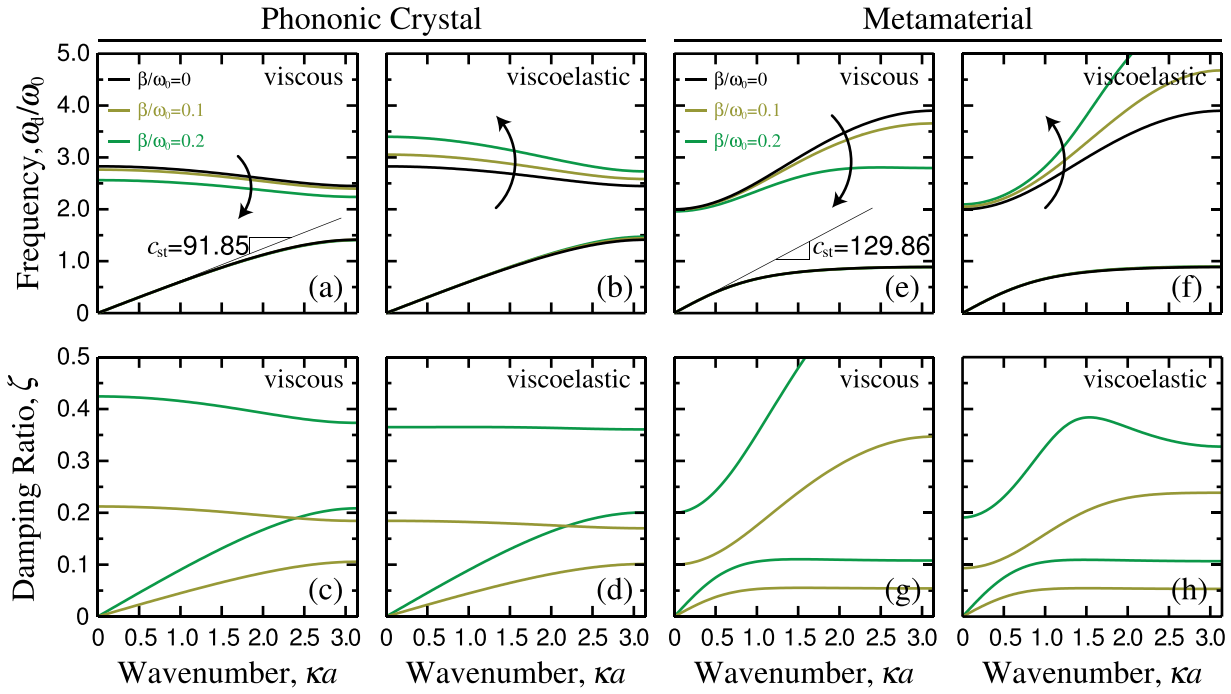

FIG. 3. (Color online) Damped dispersion diagrams (top row) of a discrete, two degree-of-freedom phononic crystal (left column) and acoustic metamaterial (right column). The undamped, long-wavelength speed of sound c_{st} is displayed for the viscous cases. The corresponding damping ratio diagrams (bottom row) are a consequence of a complex temporal frequency in the application of the Bloch condition. All mass, stiffness, and damping parameters are identical between each material model.

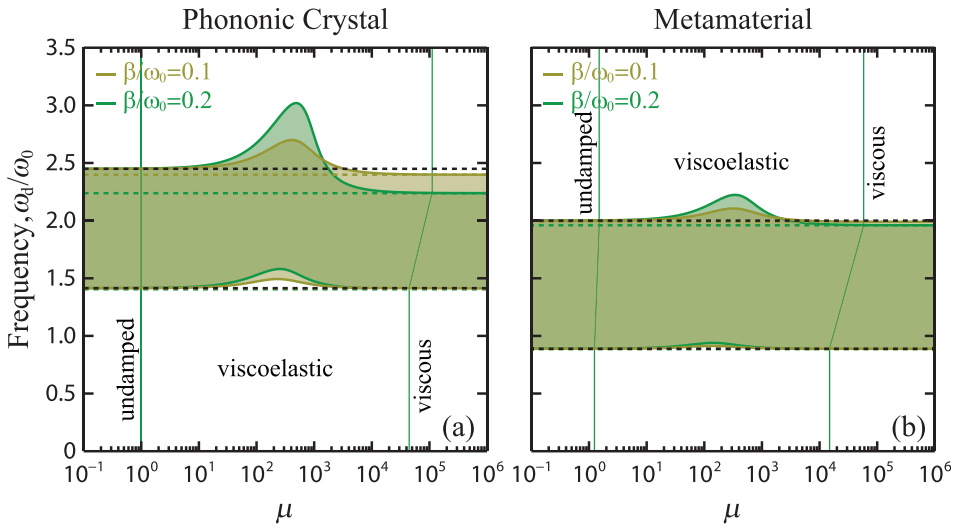

FIG. 4. Viscoelasticly damped band-gap edge frequencies over the viscoelastic-viscous regime. Dashed, horizontal lines mark the value of the corresponding undamped and viscously damped band-gap frequencies.

C. Damping zones and transition lines

In Sec. II B, we emphasized that in the limit $\mu_j \to \infty \; \forall j$, the viscous state-space formulation [Eq. (8)] is recovered. For each material configuration of the models examined in Fig. 3, the plots in Fig. 4 track the evolution of the viscoelasticly damped band-gap edge frequencies over a range of μ for $\beta/\omega_0 = 0.1$ and $\beta/\omega_0 = 0.2$. The light and dark green dashed horizontal lines indicate the location of the viscously damped edge frequencies for, respectively, these two values of damping intensities. The dashed black lines correspond to the undamped case. The maximum viscoelastic effect grows with damping intensity as the storage capability of the Maxwell element is amplified more than the dissipative capacity. The figure clearly illustrates the effects of the level and type of prescribed damping on the size and location of the band gap. It can be observed in the vicinity of $\mu = 500$, the metamaterial, similar to the phononic crystal, experiences a noticeable change in band-gap size/location.

For ease of exposition, since the results are similar between the material types, we focus exclusively on the phononic crystal model to further examine viscoelastic wave propagation. The plots in Fig. 5 highlight the viscous-viscoelastic metamorphosis particular to $\beta/\omega_0 = 0.2$ in Fig. 4(a). Using a Maxwell element with a fixed c and variable k_M as a guide, we inspect the damped band-gap edge frequencies for various values of $\mu \propto k_M$. Point A marks the value of μ at which the band-gap edge frequency is 1% over the viscous value and beyond which k_M is so stiff that it is effectively a rigid rod such that the vast majority of the energy transferred to the Maxwell element is rapidly dissipated by the dashpot (i.e., proportionally less energy is stored by the spring k_M). In this limiting case, the band structure obtained by the viscoelastic model converges with the band structure obtained by the viscous model. Conversely, point D marks the value of μ at which the band-gap edge frequency is 1% over the undamped value and below which k_M is so elastic as to effectively disengage the dashpot so as to deprive the Maxwell element of mechanical influence. As a result, the band-gap edge frequencies obtained by the viscoelastic model approach their undamped values and so does the band structure as a whole. Between points A and D, while dissipation remains present in the Maxwell element, k_M is neither too rigid nor too flexible to store a meaningful fraction of mechanical energy. Point B marks the value of μ where the undamped and damped band-gap edge frequencies are equal, as if the spring component of the Maxwell element cancels the damping component, although this equivalence is not necessarily true over the entire wavenumber domain. At point C, the energy storage capability reaches its zenith and the damped band-gap edge frequency achieves the greatest separation above its viscously damped counterpart.

In Fig. 5, it is apparent that points A–D do not coincide between the two branches, thus rendering the transition between the viscous and viscoelastic behavior frequency dependent. To better distinguish the two damping regimes, we identify essentially viscous damping as that for which the viscoelastic band structure ω_{VE} is, on average, within 1% of the viscous band structure ω_V as obtained from the matrices

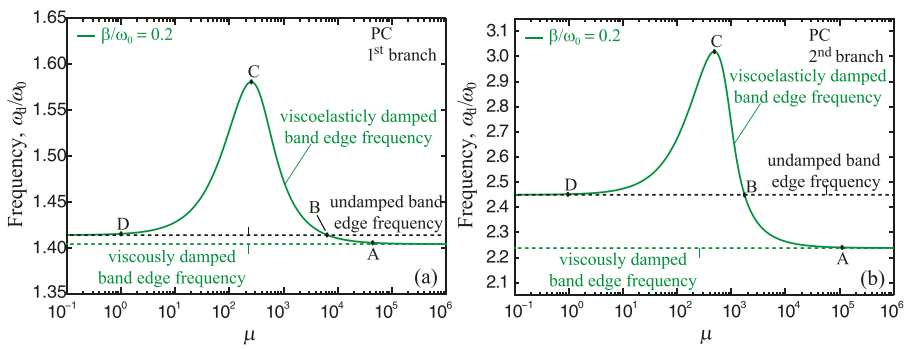

FIG. 5. (Color online) Detailed view of viscoelasticly damped band-gap frequencies in Fig. 4 ($\beta/\omega_0 = 0.2$).

of Eq. (8). Similarly, with the undamped band structure ω_U as a reference, we separate the qualitatively undamped and viscoelastic regions. Mathematically, the relevant criteria is stated as follows:

$$\phi_U = \frac{1}{mP}\sum_{s=1}^{m}\oint\left(\frac{\omega_{VE,s}}{\omega_{U,s}} - 1\right) d\kappa, \quad \begin{cases} \phi_U \le 0.01 & \text{undamped} \\ \phi_U > 0.01 & \text{viscoelastic,} \end{cases} \tag{25a}$$

$$\phi_V = \frac{1}{mP}\sum_{s=1}^{m}\oint\left(\frac{\omega_{VE,s}}{\omega_{V,s}} - 1\right) d\kappa, \quad \begin{cases} \phi_V \le 0.01 & \text{viscous} \\ \phi_V > 0.01 & \text{viscoelastic,} \end{cases} \tag{25b}$$

where P is the path length along the border of the irreducible Brillouin zone (IBZ). In the present case, assuming a lattice spacing of $a = 1$, then $P = \pi$.

Figures 6(a) and 6(b) show the variation of $\phi_{U,V}$ as a function of μ for a set of damping intensities, specifically, $\beta/\omega_0 = \{0.05, 0.10, 0.15, 0.20\}$. Figure 6(c) combines the results of Figs. 6(a) and 6(b) to define a viscoelastic region over a range of damping levels. Typically, $\phi_{U,V}(\mu)$ displays a single maximum at $\mu = \mu_{peak}$ where the band structure obtained by the viscoelastic model has the greatest disagreement with the

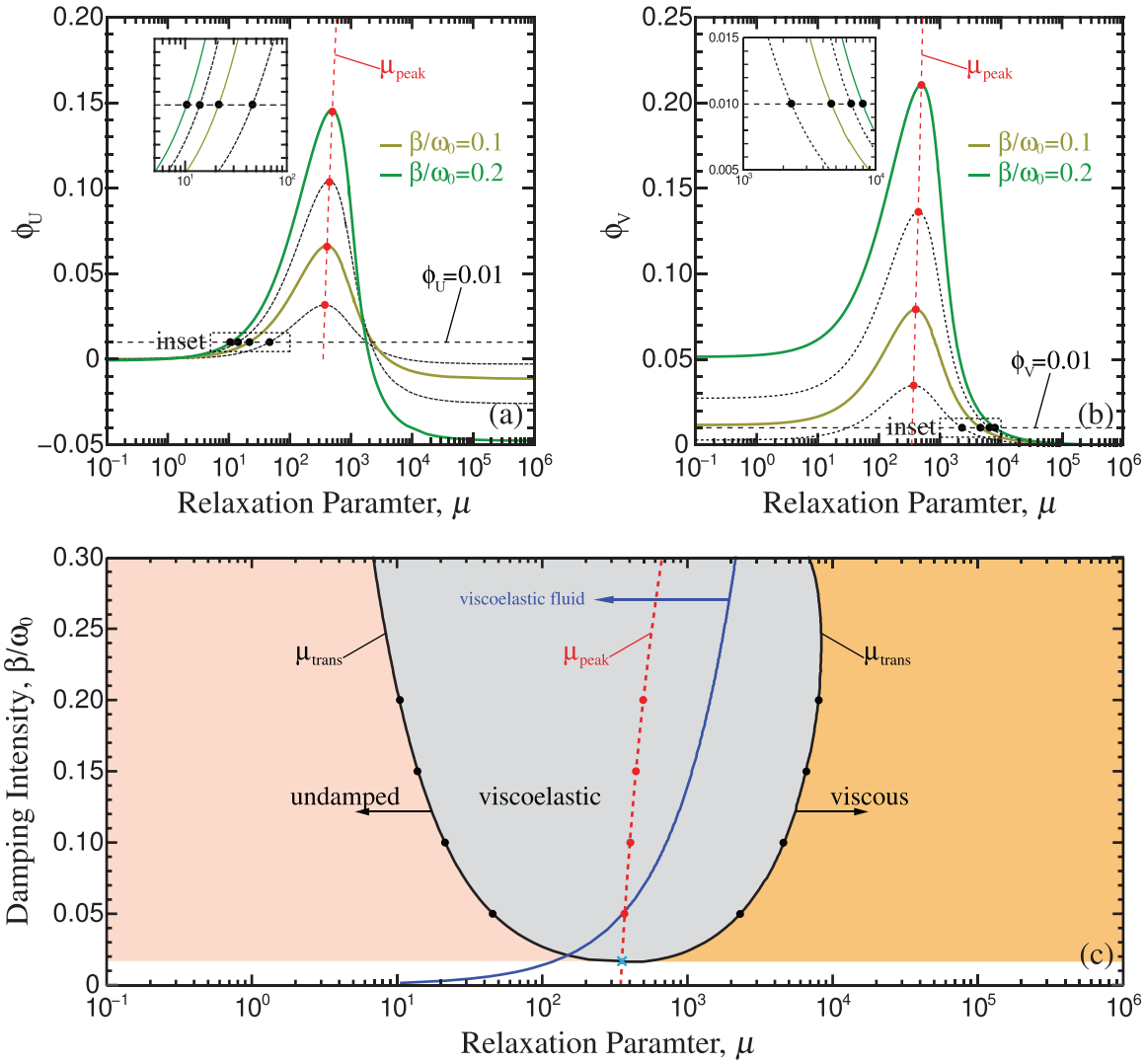

FIG. 6. The fractional deviation of the viscoelastic band structure ω_{VE} from the (a) undamped band structure ω_U and (b) viscous band structure ω_V. Particular to the damping intensity, ω_{VE} transitions to either ω_U or ω_V at a specific $\mu = \mu_{trans}$. With $\mu_{trans} < \mu_{peak}$, $\phi_U(\mu_{trans}) = 0.01$ marks the undamped-viscoelastic transition. Similarly, with $\mu_{trans} > \mu_{peak}$, the viscous-viscoelastic transition occurs when $\phi_V(\mu_{trans}) = 0.01$. (c) A map distinguishing the three phases of ω_{VE}. The viscoelastic fluid domain indicates where wave propagation is possible even with $\mathbf{K} = \mathbf{0}$.

relevant band structure. In Fig. 6(a), for $\mu < \mu_{peak}$, ϕ_U approaches zero as ω_{VE} better approximates ω_U. Detailed in the inset, the undamped-to-viscoelastic transition occurs at $\mu = \mu_{trans}$, where $\phi_U(\mu_{trans}) = 0.01$. As the prescribed damping intensity β/ω_0 increases, it is observed that μ_{trans} shifts to ever lower values. Above μ_{peak}, the function converges to negative values as ω_{VE} descends below the undamped band structure to approach ω_V. Using ϕ_V, Fig. 6(b) shows the transition of the band structure from viscoelastic to the viscous condition. In Fig. 6(b), as β/ω_0 increases, the slope of ϕ_V for $\mu > \mu_{peak}$ becomes steeper such that the transition to viscous behavior becomes more abrupt. At the higher damping intensities presented in Fig. 6(c), μ_{trans} indicates the increasing abrupt transition as it moves closer to μ_{peak}. Below μ_{peak}, the opposite occurs and ever smaller values of μ are required to trigger the transition to the undamped regime.

The transitions to viscoelastic behavior from the respective undamped and viscously damped conditions as a function of β/ω_0 are indicated in Fig. 6(c). Below $\beta/\omega_0 \approx 0.016$, $\phi_{U,V} \leq 0.01\ \forall\mu$ and so, following our criteria, no clear distinction between the three damping scenarios exists. However, given that undamped and viscous qualities reside on either side of μ_{peak}, it may serve as a boundary between the two regimes in this otherwise ambiguous damping region. At $\beta/\omega_0 \approx 0.016$, the viscous-viscoelastic transition is established when first $\phi_{U,V}(\mu_{peak}) = 0.01$ and $\mu_{trans} = \mu_{peak}$. Generally, for ϕ_U and ϕ_V, these points do not coincide but converge with transition criteria more strict than the present 1%.

Remarkably, for constant β/ω_0, an overly damped, nonpropagating dispersion branch [$\omega_{d,s}(\kappa) = 0$ for all or a subset of κ] in the viscous region may become a propagating branch in the viscoelastic region as a result of the amplification of k_M with decreased μ. This amplification leads to a second interesting result. Under viscous circumstances, if $\mathbf{K} = \mathbf{0}$, wave propagation is impossible; however, with the storage capability of the Maxwell element, under viscoelastic conditions, this is not necessarily true. Increasing $\mathbf{C}$ or decreasing μ may amplify k_M to the extent of supporting oscillation and, thus, wave propagation in the phononic material. With $\mathbf{K} = \mathbf{0}$ and the appropriate kernel function, we model a viscoelastic fluid,[37] not a viscoelastic solid. For our phononic crystal, the viscoelastic fluid domain (where propagation is possible despite $\mathbf{K} = \mathbf{0}$) is indicated in Fig. 6(c).

The map concept in Fig. 6(c) may be used by designers to tailor the type and intensity of damping in order to fall within the regime of interest, and thus tailor the dissipation as well as the dispersion and band-gap behavior as desired.

IV. METADAMPING: ENHANCEMENT OF MODAL DISSIPATION

A. Enhancement of modal dissipation by local resonance

To combat potentially damaging dynamic loads, it is desirable for an engineering material to possess a high damping capacity while also maintaining a load-bearing capability (stiffness). However, for conventional materials, an advantage in one of these traits usually comes at the expense of the other. For example, the load-bearing capability of steel is exploited in many engineering applications although its damping capacity is weak; on the contrary, polymers such as rubber excel at dissipating energy but possess little stiffness. Several approaches have been proposed to meet the challenge of achieving simultaneously high stiffness and high damping within a material. Chung[30] sought the optimal combination of dissipative and stiff elements forming a composite. Van Humbeek[31] explored the conditions (amplitude, frequency, etc.) for which metal alloys with highly dissipative martensitic phases achieved superior damping and stiffness. Lakes *et al.*[32] demonstrated the efficacy of embedding negative-stiffness inclusions within a supporting matrix to generate a material with extreme damping and stiffness. Meaud *et al.*[33] designed a hierarchical microstructure that displayed significantly higher stiffness than conventional polymers while maintaining high damping. In a recent study,[6] the concept of metadamping was introduced to describe the phenomenon of *damping emergence* that may arise in an acoustic/elastic metamaterial. Specifically, when compared to a statically equivalent phononic crystal with identically prescribed damping, a metamaterial may exhibit higher dissipation levels across particular modes of wave propagation. This phenomenon has implications for the design of highly dissipative materials that maintain (or do not sacrifice) mechanical load-bearing capacity. Previously, metadamping has been demonstrated for viscous conditions.[6] In this section, we utilize our material models to illuminate the metadamping phenomenon in the context of viscoelastic damping.

Given that the total mass of each configuration in Fig. 2 is the same, static equivalence is achieved when, in the absence of dissipation, the long-wavelength sound speed, $c_{st} = \lim_{\kappa\to 0}(\omega_1(\kappa)/\kappa)$, of each material is also in agreement. At present, as indicated in Figs. 3(a) and 3(e), $c_{st}^{PC} = 91.85$ and $c_{st}^{AM} = 129.86$. While maintaining r_k, the two long-wavelength sound speeds may be brought into agreement by strengthening the springs of the phononic crystal such that ω_0 is configuration-specific (i.e., $\omega_0^{PC} \neq \omega_0^{AM}$). Alternatively, the same goal can be achieved by weakening the springs of the metamaterial. The damping ratio diagrams may then be used to justly compare the damping capacity of each material configuration. For this purpose, we calculate the total damping ratio over both branches,

$$\zeta_{tot}^{\nu} = \sum_{s=1}^{m} \oint \xi_s^{\nu}(\kappa)\, d\kappa, \quad \nu = PC, AM, \tag{26}$$

where the integration is over the IBZ boundaries.

For $\beta/\omega_0 = 0.2$, the diagrams in Fig. 7 illustrate the variation of ξ_{tot} over a range of c_{st}. In each plot, the dashed curve corresponding to ζ_{tot}^{AM} and the solid curve of ζ_{tot}^{PC} enclose a positive metadamping region (i.e., $\zeta_{tot}^{AM} - \zeta_{tot}^{PC} > 0$). A typical feature of each plot is the downward slope of ζ_{tot}^{ν} as c_{st} increases, a result of the material becoming stiffer. The metadamping region is bounded on the left by a minimum value of c_{st} for which dissipative wave propagation is still possible for both configurations over the entire boundary of

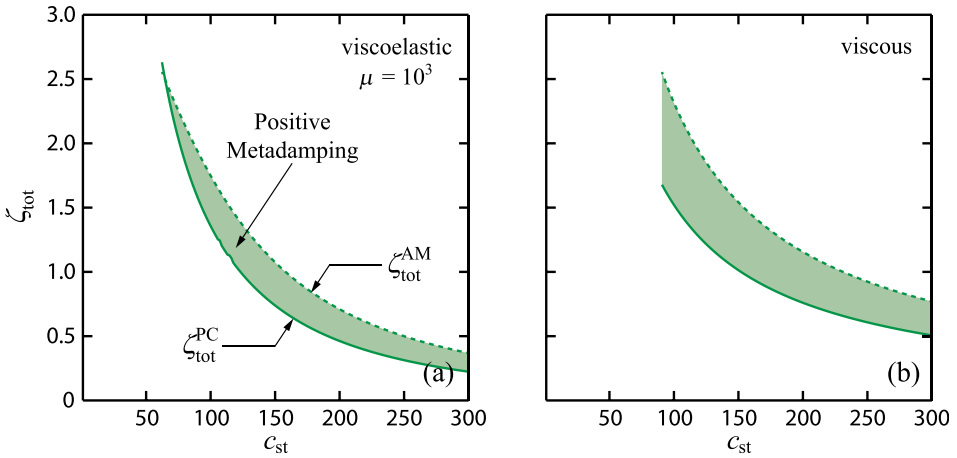

FIG. 7. (Color online) Total damping ratio over both branches for the phononic crystal (solid) and metamaterial (dashed) over a range of c_{st} values for (a) the viscoelastic condition and (b) the viscous condition. The total damping ratio of each configuration is displayed for comparison until the overdamped condition ($\zeta > 1$) is attained.

the IBZ. Below this value of c_{st}, the acoustic metamaterial is overdamped ($\zeta > 1$), but because Eq. (11) is valid for $\zeta \leq 1$, a fair comparison of ζ_{tot}^{PC} and ζ_{tot}^{AM} can no longer be made. Inspecting each frame in Fig. 7 reveals the effect of viscoelasticity on the metadamping region. Naturally, the metadamping region diminishes and favors the lower left of the diagram as the damping condition becomes more viscoelastic and heredity mitigates the dissipation of mechanical energy.

Figure 8 shows the sensitivity of the metadamping phenomenon to the relevant material parameters. As increased heredity (decreased μ) effectively transforms the viscous dampers into elastic springs in Fig. 8(a), the metadamping region simultaneously descends the ξ_{tot}-axis and collapses. Metadamping results from the concentration of strain energy, a task at which the acoustic metamaterial, with the aid of the internal resonator, outperforms the phononic crystal. In general, as illustrated in Figs. 8(b) and 8(d), decreasing r_m or increasing the coupling between m_1 and m_2 through $r_k \to \infty$ diminishes the role of the internal resonator and curtails the metadamping phenomenon. In particular, Fig. 8(b) reveals a narrow region of negative metadamping (i.e., $\zeta_{tot}^{AM} - \zeta_{tot}^{PC} < 0$). For scenarios in which the resonator mass, $m_2 \ll m_1$, the metamaterial resembles a monoatomic phononic crystal. Manipulating the ratio of damping viscosities r_c bestows the metamaterial resonator with more/less influence over the emergent phenomenon. Smaller storage ratios are indicative of a decreased ability for the metamaterial resonator to cache the energy of oscillation and, thus, the dissipative element of the resonator expresses greater

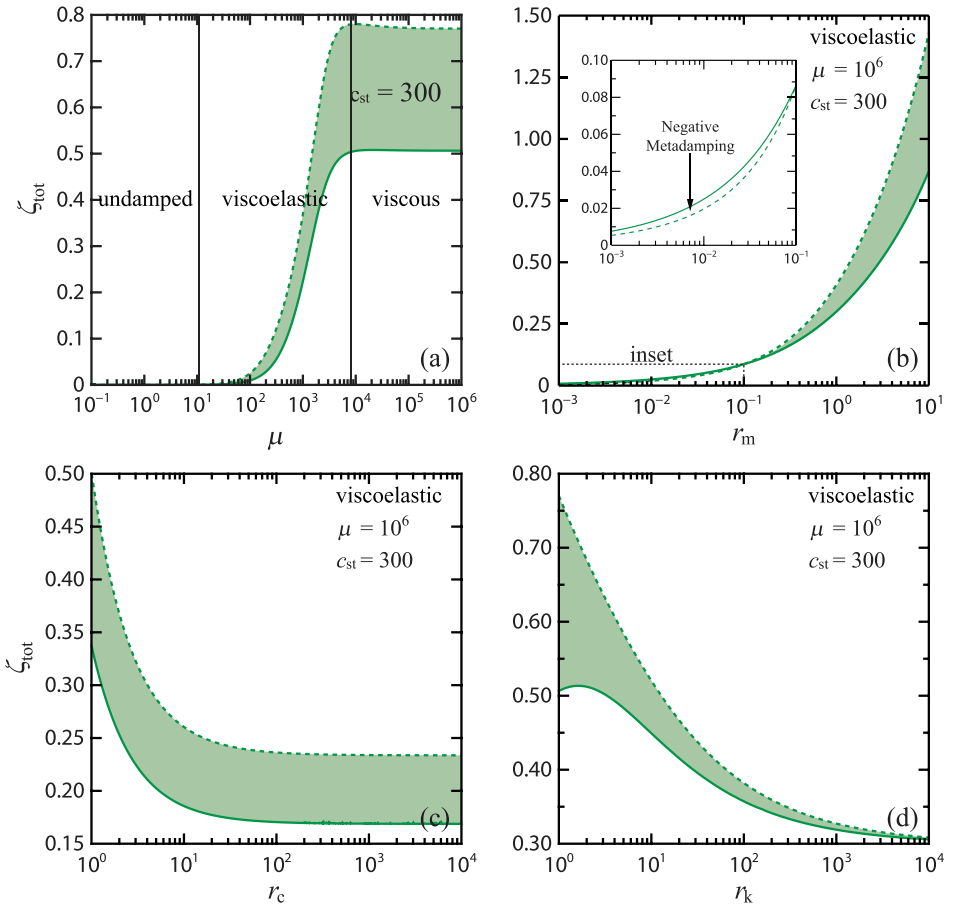

FIG. 8. (Color online) Variation of the metadamping phenomenon with material parameters r_m, r_c, and r_k affecting the influence of the metamaterial internal resonator and μ affecting the influence of heredity. Damping intensity is held constant at $\beta/\omega_0 = 0.2$. Except where plainly contradictory, $r_m = 3$, $r_c = 1/2$, and $r_k = 1$. A negative metadamping ($\zeta_{tot}^{AM} < \zeta_{tot}^{PC}$) region emerges as $r_m \to 0$.

influence. Consequently, smaller storage ratios promote the emergence of the metadamping phenomenon.

B. Effect of local resonance type

Until now, metadamping has been demonstrated with the aid of a locally resonant material possessing a dipole resonance (DP). However, locally resonant material designs featuring monopolar[41] and quadripolar[42,43] resonances appear in the literature. This motivates a study of what effect the type of resonance has on the material dissipation capacity. Continuing with the 1D lumped parameter models used thus far, in Fig. 9, we present the unit cell of an elastic metamaterial similar to that of Ref. 44 (although with damping elements) and supporting a monopole resonance (MP). Four rigid, massless truss members connect the unit cell microstructure.

While the mass and transformation matrices are the same as those defined in Eqs. (21) and (23c), respectively, the corresponding damping and stiffness matrices for the unit cell in Fig. 9 are given by Eq. (27) where $\delta = (a/D)^2$:

$$\mathbf{C} = c_2\mathbf{C}_o = c_2\begin{bmatrix} 1/r_c+\delta/2 & \sqrt{\delta} & -(1/r_c+\delta/2) \\ \sqrt{\delta}/2 & 1 & -\sqrt{\delta}/2 \\ -(1/r_c+\delta/2) & -\sqrt{\delta} & 1/r_c+\delta/2 \end{bmatrix}, \tag{27a}$$

$$\mathbf{K} = k_2\mathbf{K}_o = k_2\begin{bmatrix} 1/r_k+\delta/2 & \sqrt{\delta} & -(1/r_k+\delta/2) \\ \sqrt{\delta}/2 & 1 & -\sqrt{\delta}/2 \\ -(1/r_k+\delta/2) & -\sqrt{\delta} & 1/r_k+\delta/2 \end{bmatrix}. \tag{27b}$$

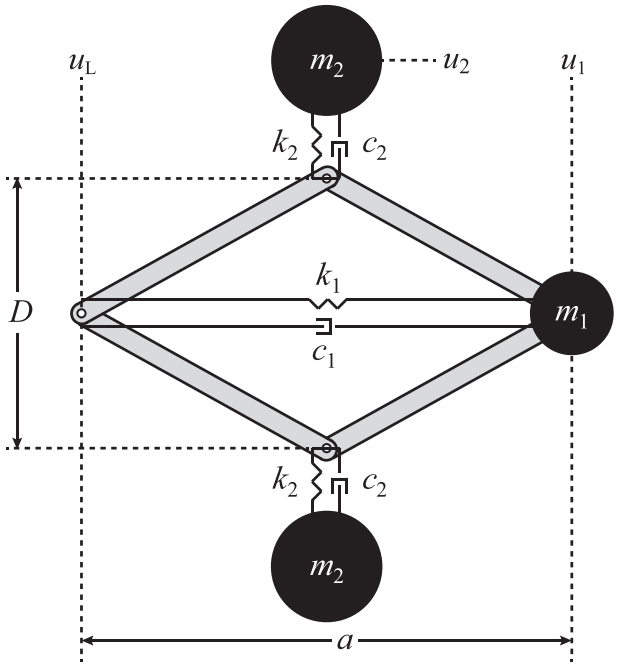

FIG. 9. Lumped parameter model of a two-phased 1D phononic material unit cell with local monopolar resonance.

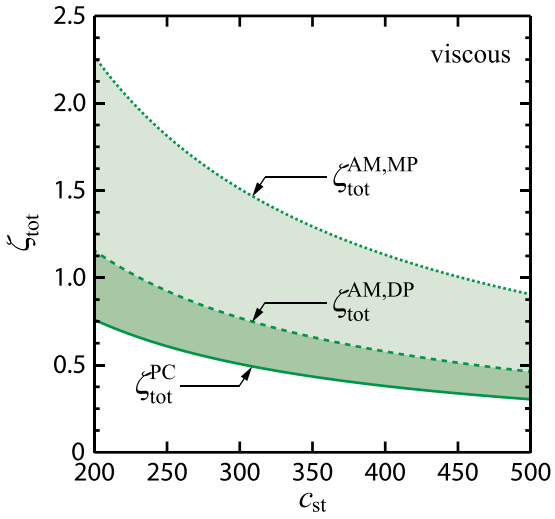

FIG. 10. (Color online) Total damping ratio over both branches for the phononic crystal (solid), metamaterial with DP (dashed), and metamaterial with MP (dotted) over a range of c_{st} values for the viscous condition.

The band structure associated with the monopolar metamaterial has features similar to the dipolar metamaterial and will not be shown here. In addition, the conclusions reached earlier in this section regarding the effects of viscoelasticity, energy concentration, and coupling on the metadamping phenomenon still hold. For brevity, we consider the viscous case in the metadamping plot in Fig. 10. Here, the total damping ratio associated with the phononic crystal, acoustic metamaterial with DP, and acoustic metamaterial with MP ($\delta = 1$) are compared over a range of c_{st}. Monopole responses have a higher degree of symmetry than those of the dipole which permits a greater concentration of mechanical energy. With the application of damping, this superior ability to pool mechanical energy results in greater dissipation amplification for the monopole metamaterial than the dipole metamaterial. Extending this reasoning to quadrupole and higher-order resonances, it is expected that the metadamping region will generally narrow with the increased order (and decreased symmetry) of the resonance. More work is needed, however, to confirm this prediction.

V. CONCLUSIONS

In this paper, the dispersion properties of phononic materials are compared when the processes of dissipation at the unit-cell level are of either viscous or viscoelastic classification, or somewhere in between. A state-space formulation of the equations of motion, extended in the case of viscoelasticity, is required to develop a representative eigenvalue problem and obtain dispersion relations. Conveniently, by changing a single parameter affecting the material relaxation, the band structure obtained by the viscoelastic model may be tuned to one of three damping regimes—undamped, viscoelastic, or viscous. When, on average, it falls outside 1% of either the undamped or pure viscous band structures, the given band structure may be designated as viscoelastic. Within the viscoelastic regime, it is shown that the effects of damping on band-gap size is generally higher in a phononic crystal compared to a locally resonant metamaterial. While viscous

dissipation contracts an existing band gap, the heredity effect of viscoelastic dissipation mitigates this response and even enlarges the band gap. These behaviors suggest that dispersion engineering may effectively be realized via dissipation engineering.

Furthermore, similar to Ref. 6, we find the influence of dissipation to be greatly affected by the configuration of the material through which a wave propagates. The metadamping phenomenon describes the enhanced damping capacity of a locally resonant material compared to a statically equivalent Bragg-scattering material. Using mechanical models of a phononic crystal and an acoustic metamaterial as characteristic Bragg scattering and locally resonant materials, respectively, metadamping is shown to diminish under viscoelastic conditions. However, due to the nature of mechanical energy localization, material systems featuring monopolar resonance exhibit metadamping more than their counterparts with dipolar resonance. The consequences of these findings extend to the design of material systems for elastic/acoustic vibration reduction, mitigation, and absorption purposes.

ACKNOWLEDGMENT

This material is based upon work supported by the National Science Foundation Graduate Research Fellowship under Grant No. DGE 1144083, the National Science Foundation CAREER Grant No. 1254931, and the Department of Education GAANN program.

[1]M. I. Hussein, M. J. Leamy, and M. Ruzzene, "Dynamics of phononic materials and structures: Historical origins, recent progress, and future outlook," Appl. Mech. Rev. **66**, 040802 (2014).
[2]M. M. Sigalas and E. N. Economou, "Elastic and acoustic wave band structure," J. Sound Vib. **158**, 377–382 (1992).
[3]M. S. Kushwaha, P. Halevi, L. Dobrzynski, and B. Djafari-Rouhani, "Acoustic band structure of periodic elastic composites," Phys. Rev. Lett. **71**, 2022–2025 (1993).
[4]Z. Liu, X. Zhang, Y. Mao, Y. Y. Zhu, Z. Yang, C. T. Chan, and P. Sheng, "Locally resonant sonic materials," Science **289**, 1734–1736 (2000).
[5]A. Sukhovich, L. Jing, and J. H. Page, "Negative refraction and focusing of ultrasound in two-dimensional phononic crystals," Phys. Rev. B **77**, 014301 (2008).
[6]M. I. Hussein and M. J. Frazier, "Metadamping: An emergent phenomenon in dissipative metamaterials," J. Sound Vib. **332**, 4767–4774 (2013).
[7]Y. Yong and Y. K. Lin, "Propagation of decaying waves in periodic and piecewise periodic structures of finite length," J. Sound Vib. **129**, 99–118 (1989).
[8]M. P. Castanier and C. Pierre, "Individual and interactive mechanisms for localization and dissipation in a mono-coupled nearly-periodic structure," J. Sound Vib. **168**(3), 479–505 (1993).
[9]E. Psarobas, "Viscoelastic response of sonic band-gap materials," Phys. Rev. B **64**, 012303 (2001).
[10]F. Bloch, "On the quantum mechanics of electrons in crystal lattices," Z. Phys. **52**, 555–600 (1929).
[11]This is in addition to the spatial decay phenomenon resulting from wave interference.
[12]J. Mead, "A general theory of harmonic wave propagation in linear periodic systems with multiple coupling," J. Sound Vib. **27**, 235–260 (1973).
[13]R. P. Moiseyenko and V. Laude, "Material loss influence on the complex band structure and group velocity in phononic crystals," Phys. Rev. B **83**, 064301 (2011).
[14]F. Farzbod and M. J. Leamy, "Analysis of Bloch's method in structures with energy dissipation," J. Vib. Acoust. **133**, 051010 (2011).
[15]E. Andreassen and J. S. Jensen, "Analysis of phononic bandgap structures with dissipation," J. Vib. Acoust. **135**, 041015 (2013).
[16]S. Mukherjee and E. H. Lee, "Dispersion relations and mode shapes for waves in laminated viscoelastic composites by finite difference methods," Comput. Struct. **5**, 279–285 (1975).
[17]M. I. Hussein, "Theory of damped Bloch waves in elastic media," Phys. Rev. B **80**, 212301 (2009).
[18]M. I. Hussein and M. J. Frazier, "Band structure of phononic crystals with general damping," J. Appl. Phys. **108**, 093506 (2010).
[19]R. Sprik and G. H. Wegdam, "Acoustic band gaps in composites of solids and viscous liquids," Solid State Commun. **106**, 77–81 (1998).
[20]X. Zhang, Z. Liu, J. Mei, and Y. Liu, "Acoustic band gaps for a two-dimensional periodic array of solid cylinders in viscous liquid," J. Phys.: Condens. Matter **15**, 8207–8212 (2003).
[21]B. Merheb, P. A. Deymier, M. Jain, M. Aloshyna-Lesuffleur, S. Mohanty, A. Berker, and R. W. Greger, "Elastic and viscoelastic effects in rubber/air acoustic band gap structures: A theoretical and experimental study," J. Appl. Phys. **104**, 064913 (2008).
[22]R. S. Langley, "On the forced response of one-dimensional periodic structures: Vibration localization by damping," J. Sound Vib. **178**, 411–428 (1994).
[23]A. S. Phani and J. Woodhouse, "Viscous damping identification in linear vibration," J. Sound Vib. **303**, 475–500 (2007).
[24]S. Phani and J. Woodhouse, "Experimental identification of viscous damping in linear vibration," J. Sound Vib. **319**, 832–849 (2009).
[25]S. Adhikari and A. S. Phani, "Experimental identification of generalized proportional viscous damping matrix," J. Vib. Acoust. **131**, 011008 (2009).
[26]S. Adhikari and J. Woodhouse, "Identification of damping: Part 1, viscous damping," J. Sound Vib. **243**, 43–61 (2001).
[27]S. Adhikari and J. Woodhouse, "Identification of damping: Part 2, non-viscous damping," J. Sound Vib. **243**, 63–88 (2001).
[28]N. Wagner and S. Adhikari, "Symmetric state-space method for a class of nonviscously damped systems," AIAA J. **41**, 951–956 (2003).
[29]J. Woodhouse, "Linear damping models for structural vibration," J. Sound Vib. **215**, 547–569 (1998).
[30]D. L. Chung, "Structural composite materials tailored for damping," J. Alloys Compd. **355**, 216–223 (2003).
[31]J. Van Humbeeck, "Damping capacity of thermoelastic martensite in shape memory alloys," J. Alloys Compd. **355**, 58–64 (2003).
[32]R. S. Lakes, T. Lee, A. Bersie, and Y. C. Wang, "Extreme damping in composite materials with negative-stiffness inclusions," Nature **410**, 565–567 (2001).
[33]J. Meaud, T. Sain, B. Yeom, S. J. Park, A. B. Shoultz, G. M. Hulbert, Z.-D. Ma, N. A. Kotov, A. J. Hart, E. M. Arruda, and A. M. Waas, "Simultaneously high stiffness and damping in nanoengineered microtruss composites," ACS Nano **8**, 3468–3475 (2014).
[34]M. I. Hussein and M. J. Frazier, "Damped phononic crystals and acoustic metamaterials," in *Acoustic Metamaterials and Phononic Crystals*, edited by P. A. Deymier (Springer, New York, 2013).
[35]F. Farzbod and M. J. Leamy, "Analysis of Bloch's method and the propagation technique in periodic structures," J. Vib. Acoust. **133**, 031010 (2011).
[36]M. I. Hussein, N. Elabbasi, and L. Liu, "Finite element analysis of wave propagation in periodic Euler-Bernoulli beams," in *Proceedings of 2009 ASME International Mechanical Engineering Congress and R&D Expo*, Paper No. IMECE2009-13232, Lake Buena Vista, FL (November 13–19, 2009), CD ROM, pp. 1–7.
[37]W. Bert, "Material damping: An introductory review of mathematic measures and experimental technique," J. Sound Vib. **29**, 129–153 (1973).
[38]Y.-C. Fung and P. Tong, *Classical and Computational Solid Mechanics* (World Scientific, Singaport, 2001).
[39]In this study, we are concerned with the phenomenon of viscoelastic damping in general rather than the behavior of a particular material and so a single relaxation parameter is sufficient to demonstrate qualitative behaviors.
[40]M. I. Hussein, M. J. Frazier, and M. H. Abedinnasab, "Chapter 1: Microdynamics of phononic materials," in *Handbook of Micromechanics and Nanomechanics*, edited by S. Li and X.-L. Gao (Pan Stanford, Singapore, 2013).
[41]Y. Ding, Z. Liu, C. Qiu, and J. Shi, "Metamaterial with simultaneously negative bulk modulus and mass density," Phys. Rev. Lett. **99**, 093904 (2007).
[42]X. Ao and C. T. Chan, "Negative group velocity from resonances in two-dimensional phononic crystals," Waves Random Complex Media **20**, 276–288 (2010).
[43]Y. Lai, Y. Wu, P. Sheng, and Z.-Q. Zhang, "Hybrid elastic solids," Nature Mater. **10**, 620–624 (2011).
[44]H. H. Huang and C. T. Sun, "Theoretical investigation of the behavior of an acoustic metamaterial with extreme Young's modulus," J. Mech. Phys. Solids **59**, 2070–2081 (2011).